Supplementary Information

Spontaneous linker-free binding of polyoxometalates on nitrogen-doped carbon nanotubes for efficient water oxidation

Gil Yong Lee,‡[abc] Insu Kim,‡[b] Joonwon Lim,[abc] Moon Young Yang,[c] Dong Sung Choi,[abc] Yujin Gu,[b] Youngtak Oh,[abc] Seok Hun Kang,[abc] Yoon Sung Nam[bc] and Sang Ouk Kim*[abc]*

[a.] National Creative Research Initiative Center for Multi-Dimensional Directed Nanoscale Assembly, KAIST, Daejeon 34141, Republic of Korea
[b.] Department of Materials Science and Engineering, KAIST, Daejeon 34141, Republic of Korea
[c.] KAIST Institutes for the NanoCentury, KAIST, Daejeon 34141, Republic of Korea

‡These authors contributed equally to this work

*Corresponding authors, e-mails: sangouk.kim@kaist.ac.kr (S.O.K.) and yoonsung@kaist.ac.kr (Y.S.N.); phone: +82-42-350-3339 (S.O.K.) and +82-42-350-3311 (Y.S.N.); and fax: +82-42-350-3310

This file includes:

Experimental Section

Synthesis of tetracobalt-based polyoxometalates (Co_4POMs): $Na_2WO_4{\cdot}2H_2O$ (35.62 g, Sigma-Aldrich, St. Louis, MO, USA), $NaHPO_4{\cdot}7H_2O$ (3.22 g, Sigma-Aldrich), and $Co(NO_3)_2{\cdot}6H_2O$ (6.98 g, Sigma-Aldrich) were mixed in 35 mL of deionized water in a 100 mL round-bottom flask with magnetic stirring at 200 rpm for 20 min. The pH was adjusted to 7 by adding 5 M HCl. Deionized water was added to the prepared solution to make a total volume of 50 mL. This mixture was refluxed at 100 °C for 2 h with magnetic stirring at 200 rpm. After reflux, the mixture was cooled down to room temperature. Insoluble blue precipitates were removed by vacuum filtration (HAWP04700, MF-Millipore, Darmstadt, Germany). The filtrates were saturated with 10 g of NaCl and incubated at 4 °C overnight. The resulting deep blue-purple crystals were collected and washed with 10 mL of cooled deionized water.

Synthesis of N-doped carbon nanotubes (NCNTs): Pristine MWCNTs were purchased from Hanwha Nanotech (CM-95, purity > 95 wt-%, Hanwha Chemical, Seoul, Republic of Korea). The average diameter and length of the MWCNTs were 10-15 nm and < 1 μm, respectively. For purification, they were dispersed in a mixed solution of H_2SO_4 and HNO_3 for 10 h under ultra-sonication. For N-doping, the purified MWCNTs were thermally annealed at 1050 °C for 4 h under a mixture gas of Ar (40 sccm) and NH_3 (60 sccm).

Synthesis of polyethylenimince (PEI) coated CNTs (PEI/CNTs): Pristine MWCNTs were added to 3 M HNO_3 and sonicated in an ultrasonic bath for 30 min. Then, the MWCNTs were purified by refluxing at 80 °C for 24 h, rinsed with an excess amount of deionized water five times, and

dried at 80 °C overnight. The purified MWCNTs were dispersed in a 2 wt-% PEI aqueous solution (Mw = 2 kDa, Sigma-Aldrich). The mixed solution was stirred at 25 °C for 8 h and then rinsed with an excess amount of deionized water five times.

Synthesis of hybrids with Co_4POMs: NCNTs (5 mg) were added to a 15 mL aqueous solution (pH 5). Subsequently, an aqueous solution of Co_4POMs (20 mL, 0.5 mmol) was added into the NCNT solution. The mixture was vigorously stirred at 25 °C for 8 h. The hybrid catalysts were collected by vacuum filtration on a Millipore system (HVLP04700, MF-Millipore), and were then washed by aqueous solutions (pH 5) to remove unreacted Co_4POM molecules. The Co_4POM/CNT and Co_4POM/PEI/CNT hybrids were synthesized in the same manner using CNTs and PEI/CNTs.

Computational details: All calculations were carried out using DFT within the generalized gradient approximation (GGA) as implemented in the Vienna ab initio simulation package (VASP) code.[1] The ultrasoft pseudopotential was used with a plane wave cutoff energy of 400 eV. A periodic supercell geometry was employed to model the Co_4POM/graphene system, and the cell size was $17.02 \times 24.56 \times 30.00$ Å^3. One k point was used for the Brillouin-zone integrations. After the geometry optimizations, all the atomic forces were less than 0.05 eV/ Å. Binding energies were calculated by the following equation. $E_{binding} = E_{total} - E_{catalyst} + E_{graphene}$, where E_{total}, $E_{catalyst}$, and $E_{graphene}$ are the system energies that contain the Co_4POM on the graphene layer, the Co_4POM, and the graphene layer, respectively.

Electrochemical analysis: Five milligrams of the Co_4POMs, CNTs, PEI/CNTs, NCNTs, Co_4POM/CNT hybrids, Co_4POM/PEI/CNT hybrids, and Co_4POM/NCNT hybrids and 16 μL of a Nafion solution were dispersed in a 3:1 mixture of water and ethanol at 5 wt-% to prepare electrode inks.[2] After sonication for 30 min, 20 μL of inks were loaded onto a glassy carbon electrode that was 5 mm in diameter. All the electrochemical measurements were performed using a three-electrode system with an electrochemical station (Bio-Logic SP-200, Claix, France). An Ag/AgCl (in saturated KCl) electrode and Pt wires were used as the reference and counter electrodes, respectively. The electrochemical measurements were conducted in 80 mL of 0.1 M sodium phosphate buffer (pH 7). In 0.1 M sodium phosphate buffer (pH 7), E (RHE) = $E_{Ag/AgCl}$ + 0.059 pH + $E^0_{Ag/AgCl}$ ($E^0_{Ag/AgCl}$ = 0.197 (V) at 25 °C). All Potentials converted versus reversible hydrogen electrode (RHE). CV was conducted at a scan rate of 25 mV s^{-1}, and a potential between 0.61 and 2.21 V *vs.* RHE. LSV was also conducted at a scan rate of 5 mV s^{-1} under the same potential range. EIS analysis was conducted using the same configuration. The working electrode was biased at 1.71 V *vs.* RHE from 20 kHz to 10 mHz with an amplitude of 5 mV.

Electrolysis of water: Electrolysis was conducted in a two-compartment cell with mass cylinders and a Nafion-coated glass frit junction in a three-electrode configuration. The working electrode was prepared by depositing the samples on a glassy carbon electrode, and the Ag/AgCl reference electrode was placed near a working electrode, and a Pt wire counter electrode was placed in mass cylinders in each vessel. The chambers and mass cylinders were filled with electrolytes. Electrolysis was carried out at 2.01 V *vs.* RHE.

Characterizations: TEM, HRTEM, HAADF-STEM, and EDS mapping analysis were conducted using a Titan cubed G2 60-300 microscope (FEI, Hillsboro, Oregon, USA) operated at 80 kV. The EDS mapping was performed using a FEI Super-X detector (four symmetrically arranged silicon drift detectors). For TEM analysis, the sample was prepared by drop casting and drying the Co_4POM/CNT hybrids and Co_4POM/NCNT hybrid solutions onto a lacey carbon grid. The absorption spectra were measured using UV-Vis spectrophotometry (Shimadzu UV-2600, Kyoto, Japan). The surface charges of the Co_4POMs and NCNTs were characterized by zeta potential measurements (ELS-Z2, Hirakata, Japan). The characterization of Co_4POMs, NCNTs and the Co_4POM/NCNT hybrids was performed using XPS (Thermo Scientific, K-alpha, MA, USA), Raman spectroscopy (Horiba Jobin Yvon, Lille, France), and FT-IR (Bruker IF66/S and Hyperioin 3000, Billerica, MA, USA). The Co_4POMs deposited on NCNTs were analyzed using TGA (METTLER TOLEDO TGA/DSC 1, Greifensee, Switzerland) and ICP-MS (Agilent Technologies 7700S, Santa Clara, CA, USA). Gas chromatography (YL6500GC, YL Instrument, Anyang, Republic of Korea) analysis was conducted to determine the amount of evolved oxygen gases. Argon carrier gas, a MolSieve 5Å column, and a thermal conductivity detector were used for the analysis of oxygen.

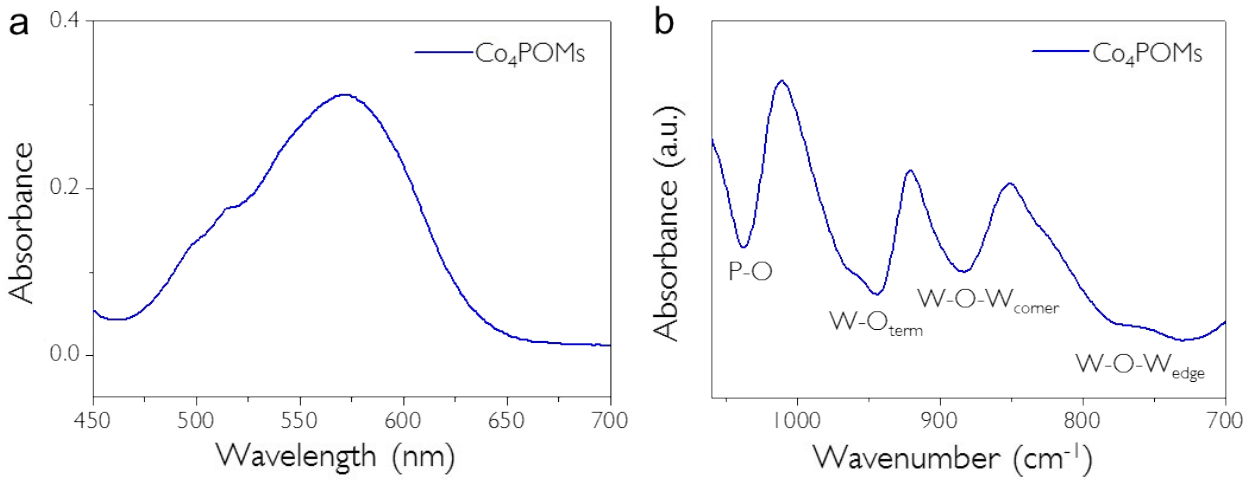

Fig. S1 (a) UV-visible absorption spectrum of 2 mM Co_4POMs in 50 mM sodium phosphate at pH 8. The max absorbance is 578 nm. (b) A series of characteristic FT-IR bands of Co_4POMs at P-O stretching (1037 cm^{-1}), terminal W-O stretching (943.9 cm^{-1}), corner W-O-W bending (884.2 cm^{-1}), and edge W-O-W bending (731.8 cm^{-1}). FT-IR spectroscopy was conducted using 1 wt-% sample in KBr pellets.

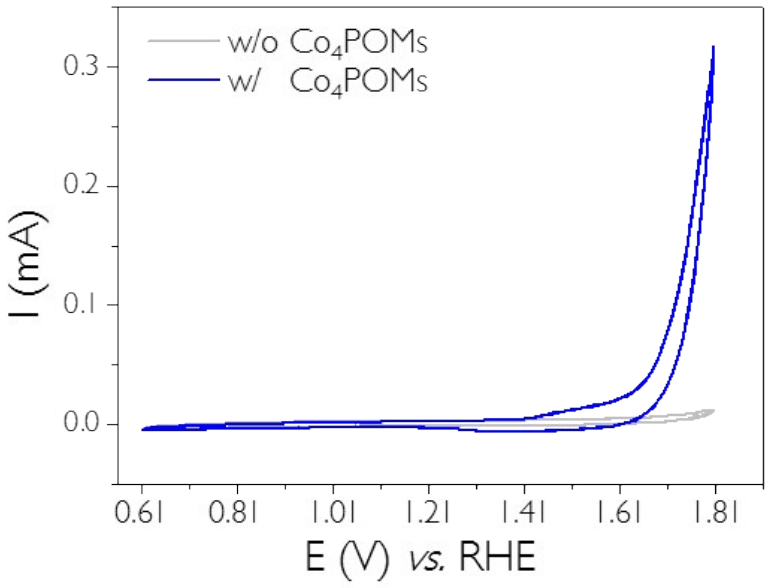

Fig. S2 Cyclic voltammogram (CV) of 0.1 M sodium phosphate at pH 7 without Co_4POMs (gray) and with 1 mM Co_4POMs (blue). Scan rate is 25 mV s^{-1}.

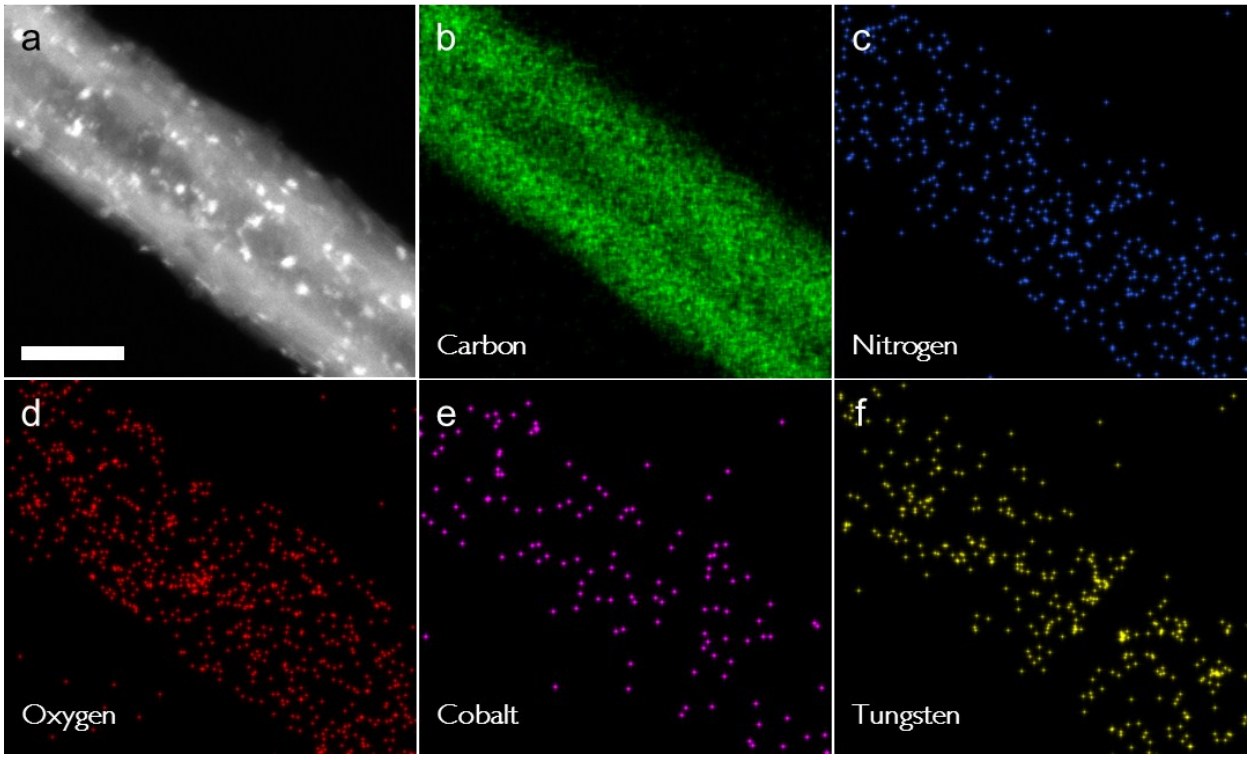

Fig. S3 (a) Z-contrast high-angle annular dark-field (HAADF) TEM image. EDS elemental mapping of $K\alpha_1$ emission of carbon (b, green), $K\alpha_1$ emission of nitrogen (c, blue), $K\alpha_1$ emission of oxygen (d, red), $K\alpha_1$ emission of cobalt (e, purple), and $L\alpha_1$ emission of tungsten (f, yellow) of the Co_4POM/NCNT hybrids; Scale bar, 10 nm.

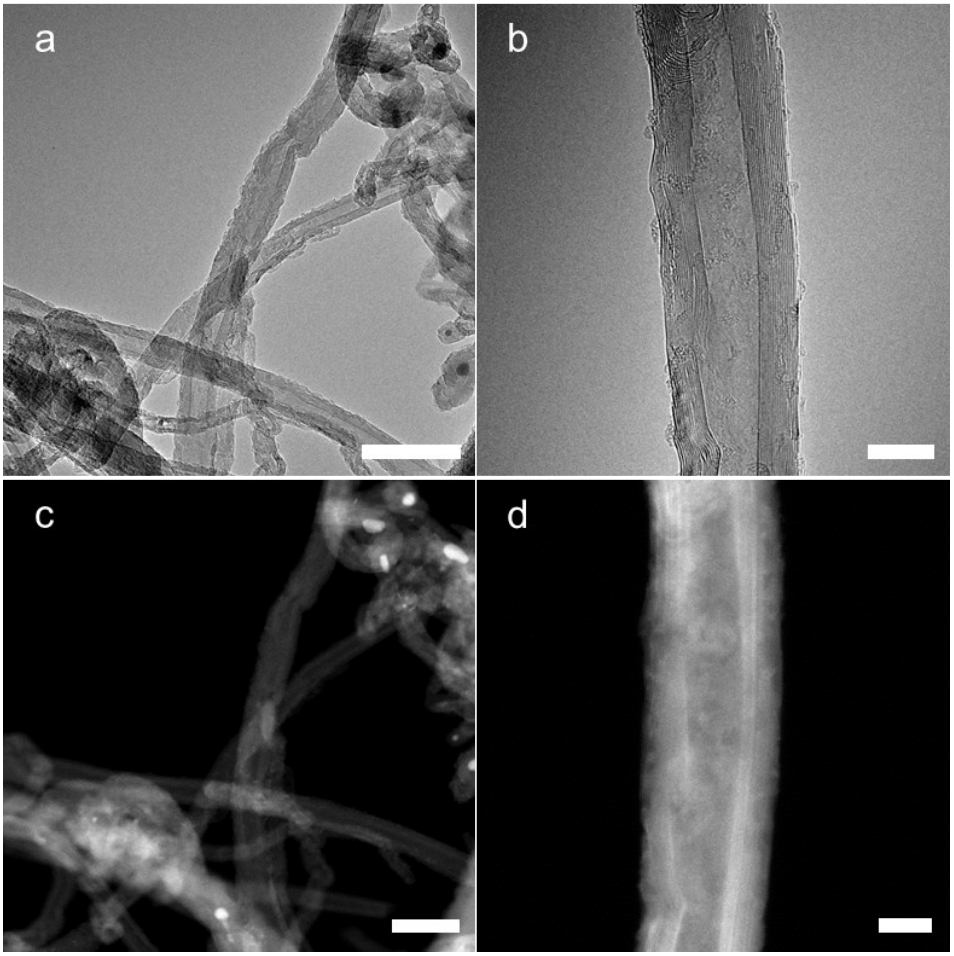

Fig. S4 (a, b) HR-TEM and (c, d) Z-contrast HAADF-TEM images of the Co_4POM/CNT hybrids prepared using pristine CNTs; Scale bar, 50 nm (a, c) and scale bar, 10 nm (b, d).

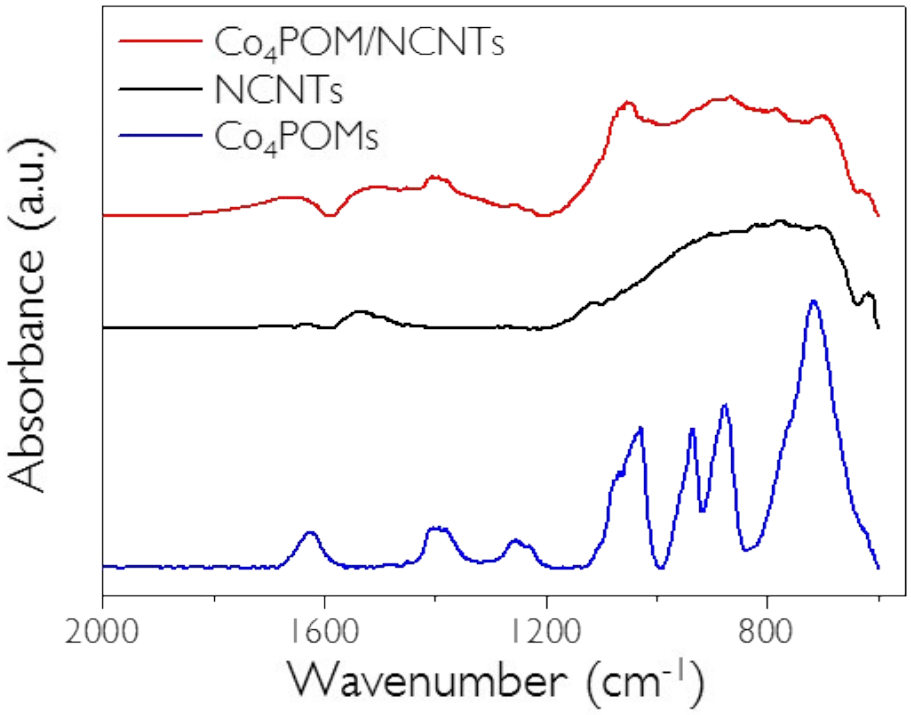

Fig. S5 Fourier transform infrared (FT-IR) spectroscopy carried out for Co_4POMs (blue), NCNTs (black), and the Co_4POM/NCNT hybrids (red). FT-IR bands of Co_4POMs (1037 ~ 731.8 cm^{-1}) were detected in that of Co_4POM/NCNT hybrids, which is not shown in NCNTs. FT-IR spectroscopy was conducted using 1 wt-% sample in KBr pellets.

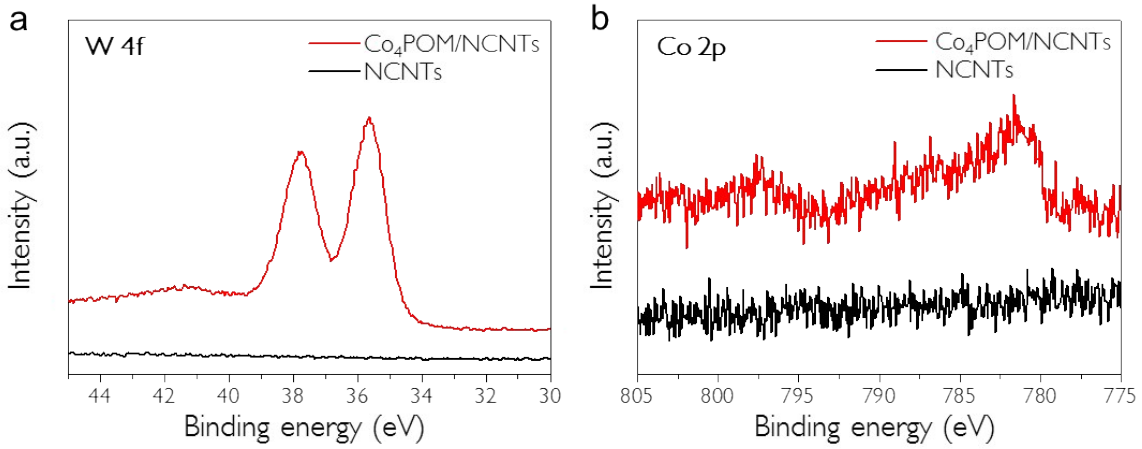

Fig. S6 (a) W3d and (b) Co2p XP spectra of the NCNTs (black) and Co_4POM/NCNT hybrids (red).

Table S1. The content of nitrogen (N) in the NCNTs and Co_4POM/NCNT hybrids. All types of N were analyzed by XPS (Fig 2C).

N content	NCNT (at-%)	Co_4POM/NCNT (at-%)
Pyridinic N (N1)	1.09	0.68
Pyrrolic N (N2)	0.21	0.25
Quaternary N (N3)	0.20	0.22
Oxidized N (N4)	0.10	0.11

The total amount of N content in NCNT is 1.60 at-%, including pyridinic nitrogen (N1) of 1.09 at-%, pyrrolic nitrogen (N2) of 0.21 at-%, quaternary nitrogen (N3) of 0.20 at-%, and oxidized nitrogen (N4) of 0.10 at-%, respectively. After hybridization, the amount of pyridinic nitrogen (N1) decreased to 0.68 at-%, while others (N2, N3, and N4) have negligible changes. According to our DFT calculation, 4N-2H$^+$ sites, composed with 4 pyridinic N, strongly attract Co_4POMs (Fig 3C). From the calculation, we assumed that 1 POM molecule adsorbs onto 4 pyridinic N. With the assumption, the theoretical amount of Co_4POMs hybridized with NCNTs are 28.1 wt-%, as follows:

$$W_{Co_4POM} = \left[\frac{A_{Co_4POM} M_{Co_4POM}}{A_{Co_4POM} M_{Co_4POM} + \left(100 - A_{Co_4POM}\right) M_{Carbon}} \right] \times 100$$

W_{Co_4POM}: wt-% of Co_4POMs
A_{Co_4POM}: at-% of Co_4POMs
M_{Co_4POM}: molecular weight of Co_4POM
M_{Carbon}: molecular weight of carbon

In our experiment, the TGA result shows 21.5 wt-% of Co_4POMs (Fig 2D). This gap is elucidated as follows: some pyridinic N in NCNT can exist in other chemical forms (4N-1H$^+$, 3N, 2N, and so on) rather than 4N-2H$^+$.

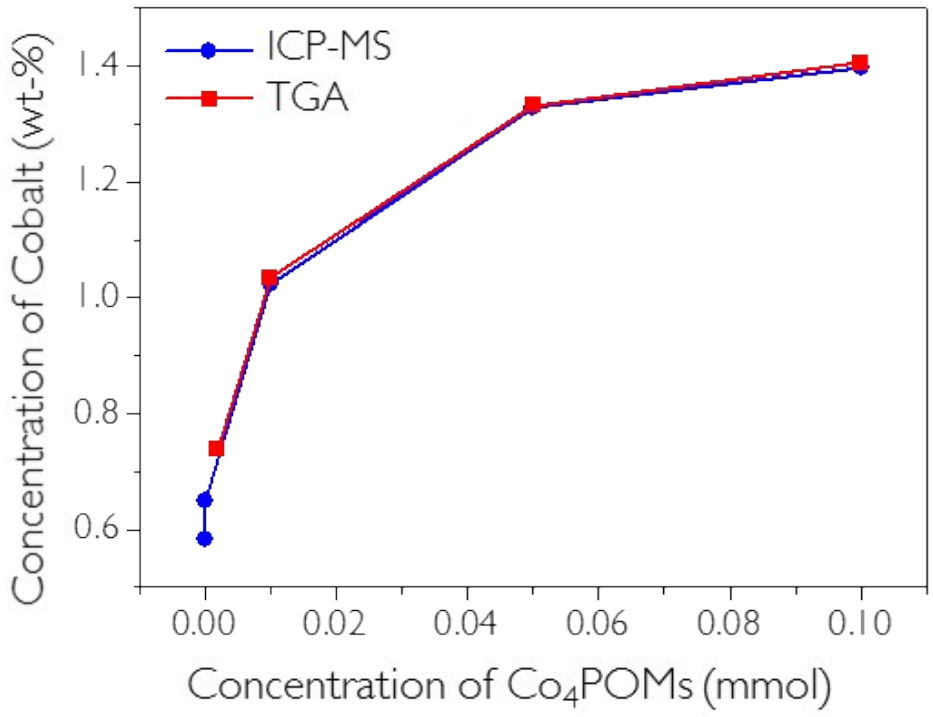

Fig. S7 ICP-MS (blue) and TGA (red) results of the concentration of cobalt in the Co_4POM/NCNT hybrids as a function of concentration of Co_4POMs for synthesis.

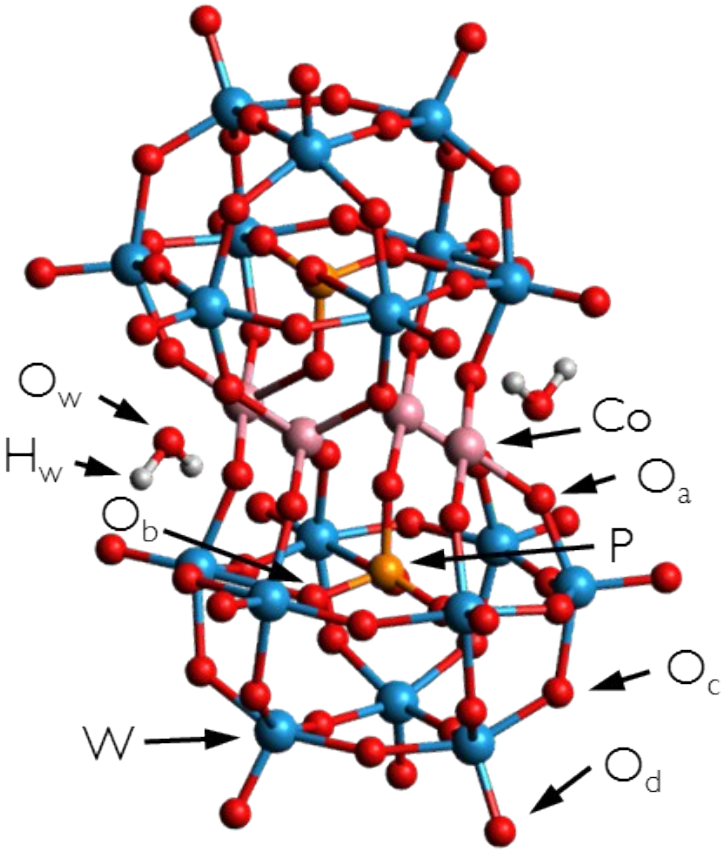

Fig. S8 Chemical structure of the Co_4POMs. Red, cyan, orange, pink, and white balls represent oxygen, tungsten, phosphorous, cobalt, and hydrogen atoms, respectively.

Table S2. The average bond lengths between two elements in the Co_4POMs. The experimental values were taken from previously reported literature.[3]

Distance (Å)	Theory	Experiment
Co - O_a	1.87	1.88
Co - O_w	1.98	1.99
P - O_b	1.53	1.54
W - O_c	1.94	1.94
W - O_d	1.74	1.74
O_w - H_w	1.00	1.00

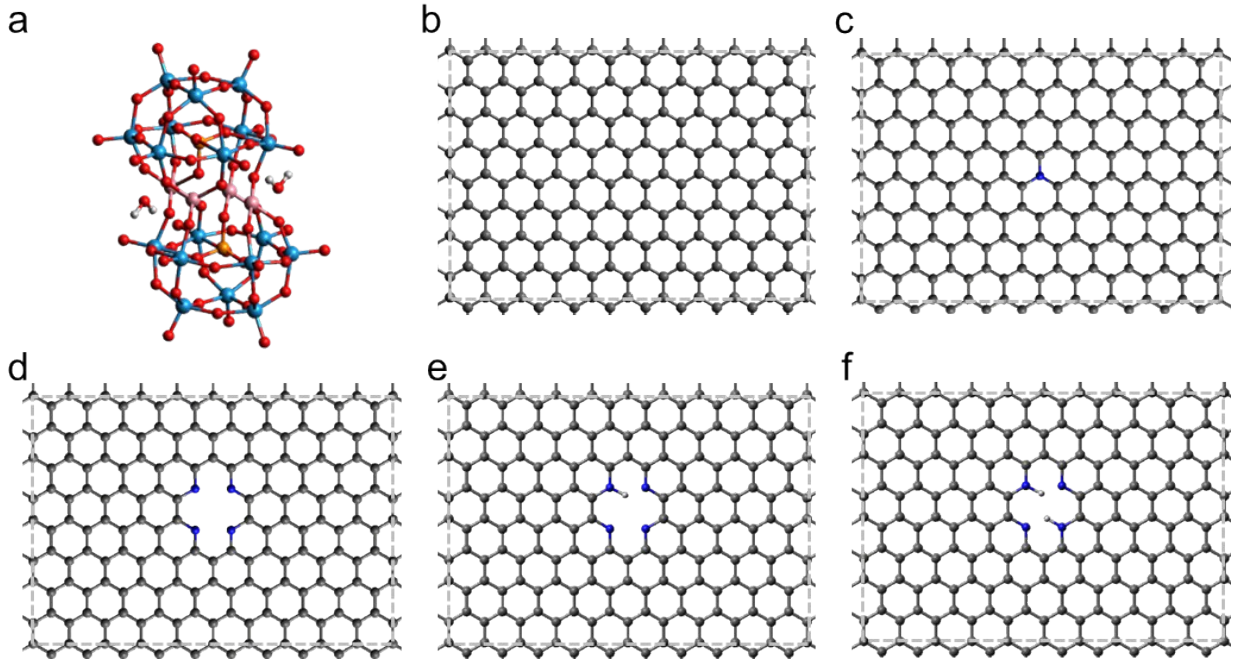

Fig. S9 The calculation models of the Co_4POMs and CNT surface. (a) Side view of Co_4POM. Top view of the graphene layers that contain (b) N-free, (c) a graphitic N atom, (d) four pyridinic N atoms with (e) one and (f) two protonated sites.

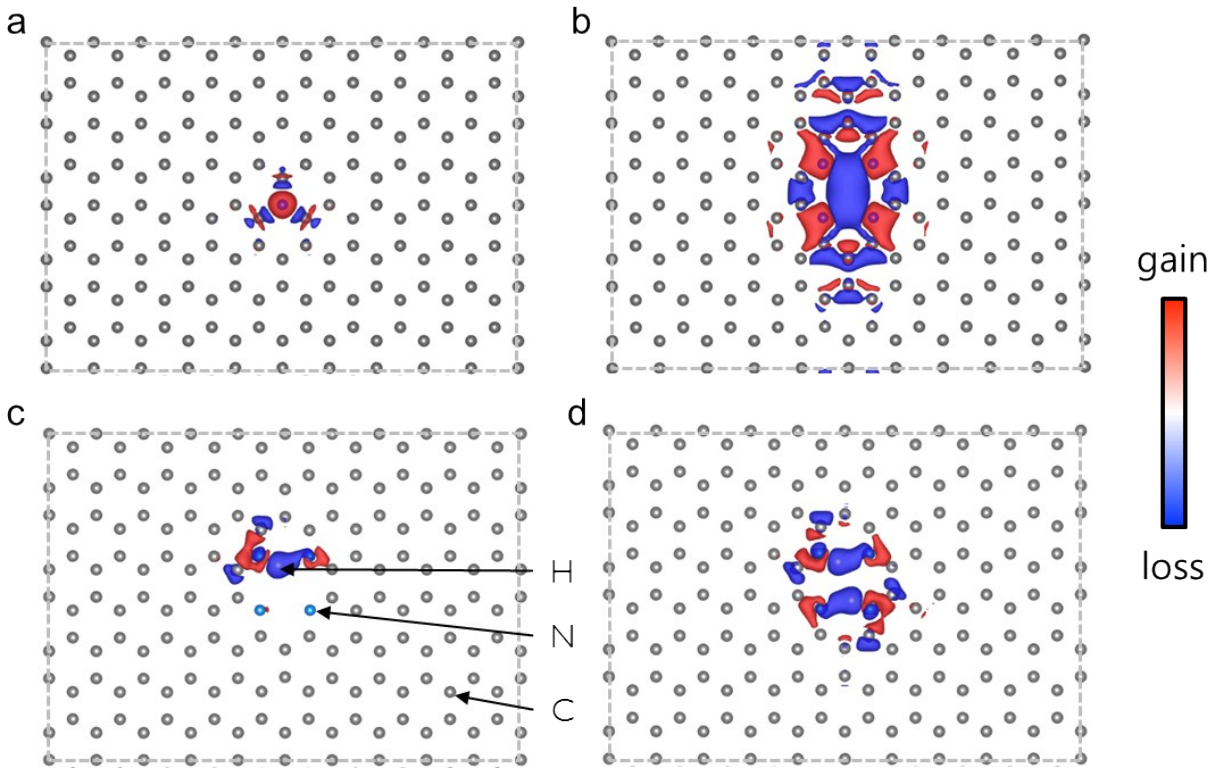

Fig. S10 Charge density difference (CDD) plots for graphene layers. (a) a graphitic N atom, (b) four pyridinic N atoms, and four pyridinic N atoms with (c) one protonated site and (d) two protonated sites. The CDDs are taken relative to the pristine graphene layer for (a) and (b) ($\Delta\rho$ = ρ (N-doped graphene) − ρ (pristine graphene)), and the four pyridinic N atoms doped graphene for (c) and (d) ($\Delta\rho$ = ρ (N-doped with protonation graphene) − ρ (N-doped graphene)).

Table S3. Average net charge of atoms in Co_4POM calculated by Bader charge analysis.[4]

Atoms	Net charge
Terminal O atoms bonded to one W atom (O_d)	-1.83
Bridging O atoms that connect two W atom (O_c)	-1.63
Bridging O atoms that connect P and W atom (O_b)	-1.83
Bridging O atoms that connect Co and W atom (O_a)	-1.53
Co	1.45
P	5.00
W	5.09

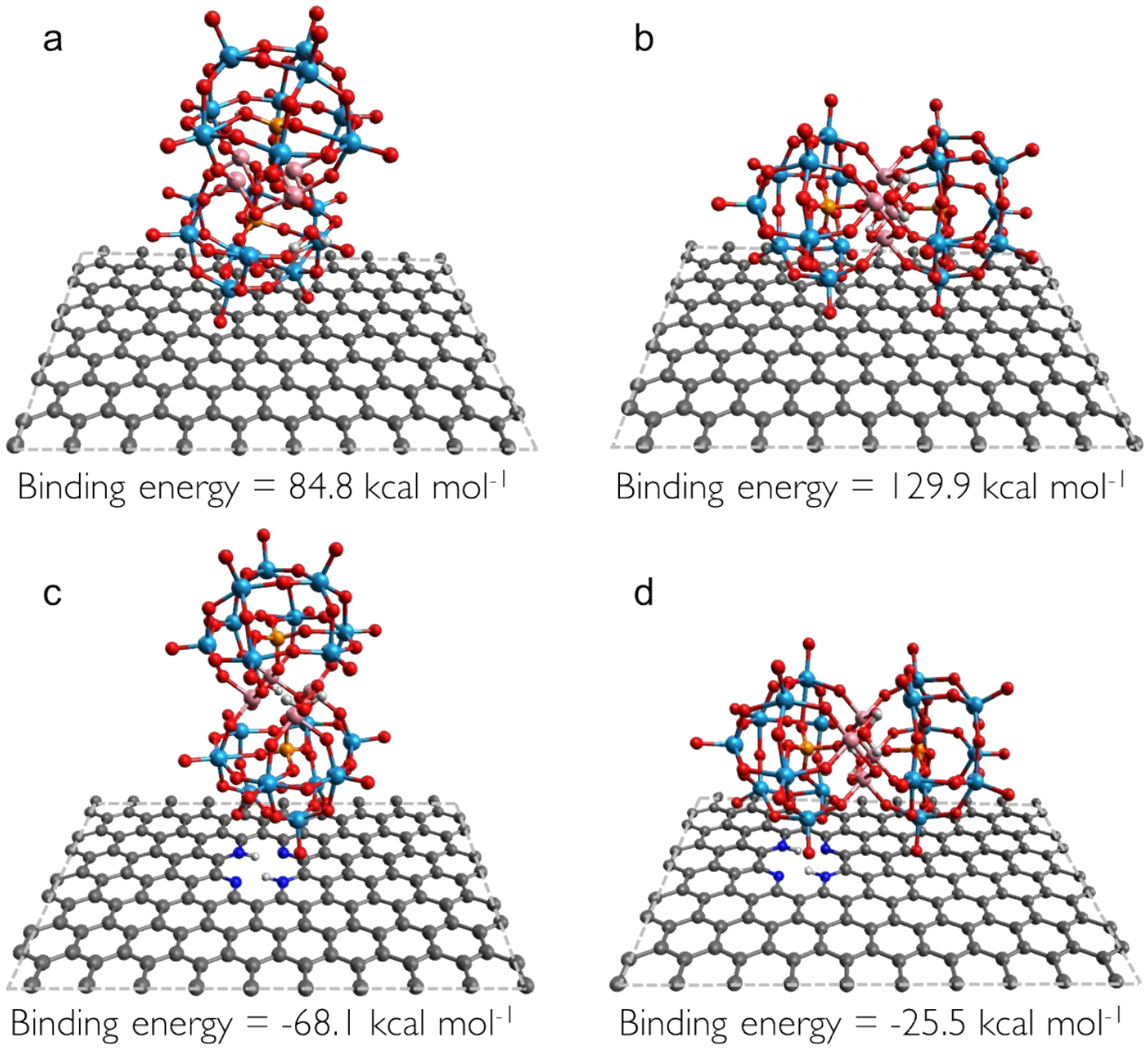

Fig. S11 Optimized structures and their binding energies of vertical (a) and horizontal (b) assemblies of the Co_4POM on the N-free graphene layers. Optimized structures and their binding energies of vertical (c) and horizontal (d) assemblies of the Co_4POM on the pyridinic 4N-2H$^+$ graphene layers.

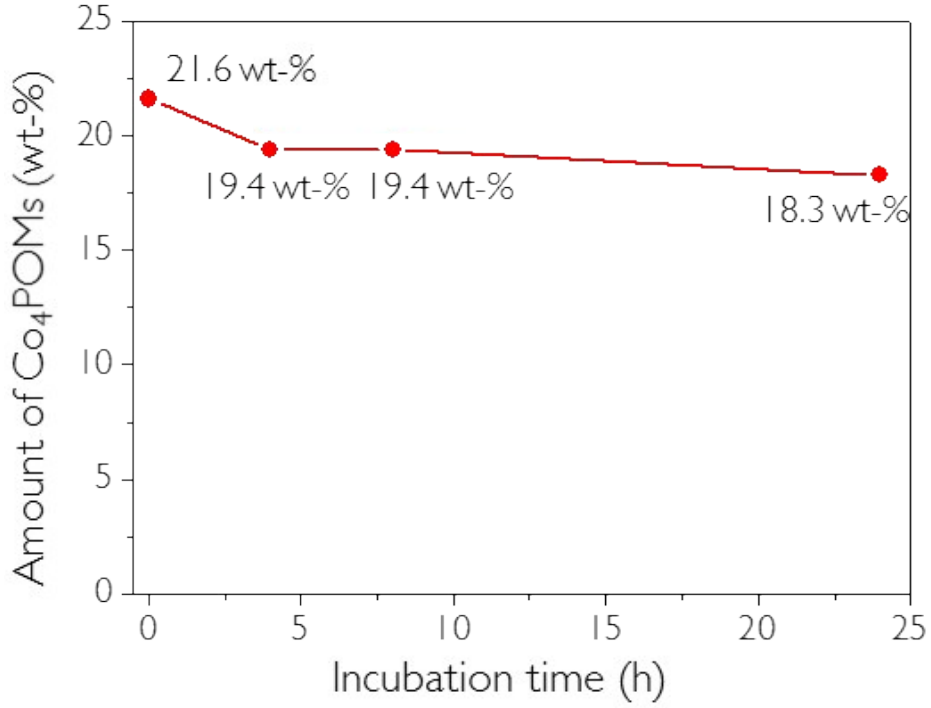

Fig. S12 The amount of residual Co_4POMs of the Co_4POM/NCNT hybrids after incubation in a buffer solution for 0, 4, 8, and 24 h at room temperature.

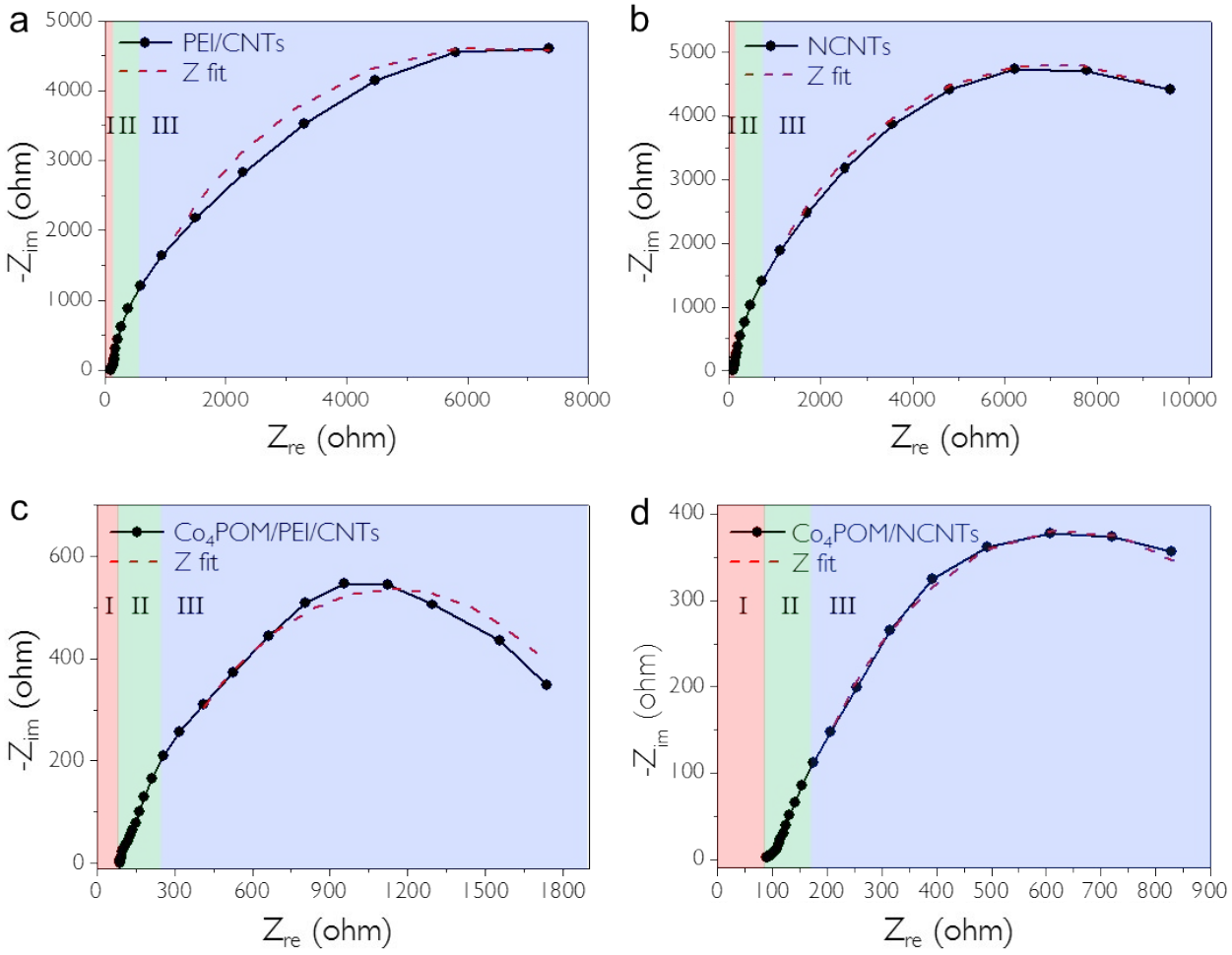

Fig. S13 The raw electrochemical impedance spectra (black) and Z fitting electrochemical impedance spectra (red) of (a) PEI/CNTs, (b) NCNTs, (c) Co_4POM/PEI/CNT hybrids, and (d) Co_4POM/NCNT hybrids at 1.1 V vs. Ag/AgCl from 5 MHz to 10 mHz. The region I, II, and III reflect ion transport through the bulk electrolyte medium, ion transport through the porous electrode, and charge transfer reaction at the electrode, respectively.

Table S4. A comparison of impedance values calculated by electrochemical impedance spectra (Fig. S13).

	R_{CT} (ohm cm^2)	Q ($Fs^{(\alpha-1)}$ cm^{-2})	α
PEI/CNTs	2430.79	3.26×10^{-3}	0.81
NCNTs	2728.32	1.99×10^{-3}	0.77
Co_4POM/PEI/CNTs	407.09	5.05×10^{-3}	0.61
Co_4POM/NCNTs	198.35	2.84×10^{-2}	0.82

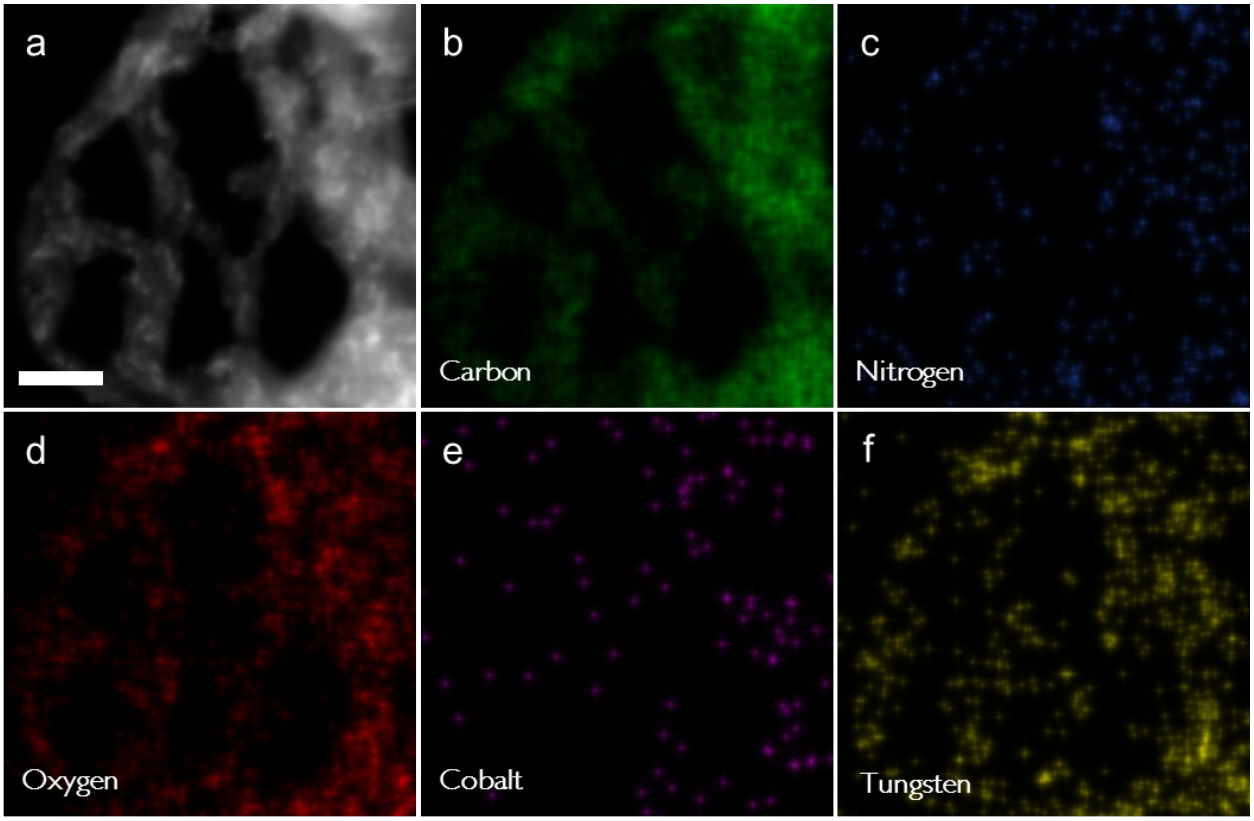

Fig. S14 (a) Z-contrast high-angle annular dark-field (HAADF) TEM image. EDS elemental mapping of $K\alpha_1$ emission of carbon (b, green), $K\alpha_1$ emission of nitrogen (c, blue), $K\alpha_1$ emission of oxygen (d, red), $K\alpha_1$ emission of cobalt (e, purple), and $L\alpha_1$ emission of tungsten (f, yellow) of the Co_4POM/NCNT hybrids after water oxidation; Scale bar, 10 nm.

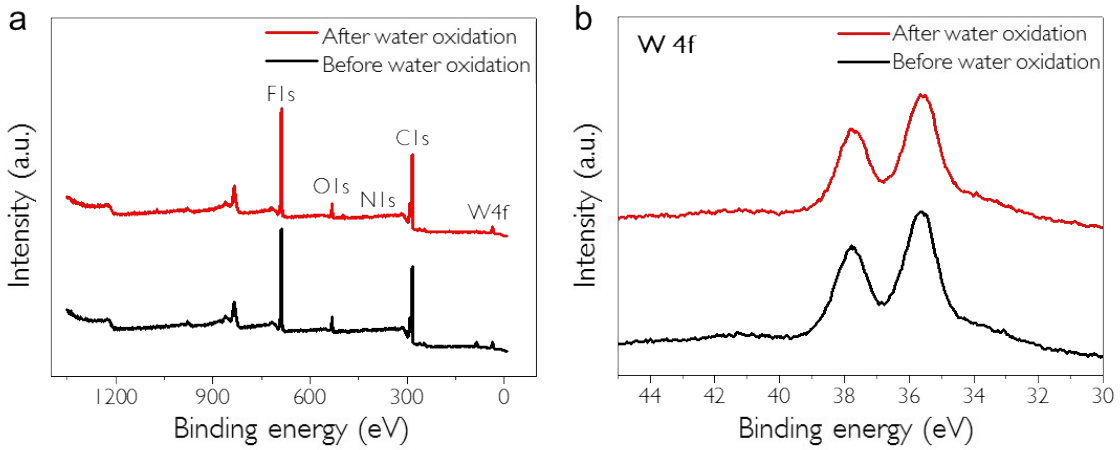

Fig. S15 (a) XPS survey spectra and (b) W 4f XP spectra of the the Co_4POM/NCNT hybrids before (black) and after (red) water oxidation. The peak intensity of W 4f was not appreciably changed before and after the reaction. It indicates that the Co_4POM/NCNT hybrids are stable during the catalysis.

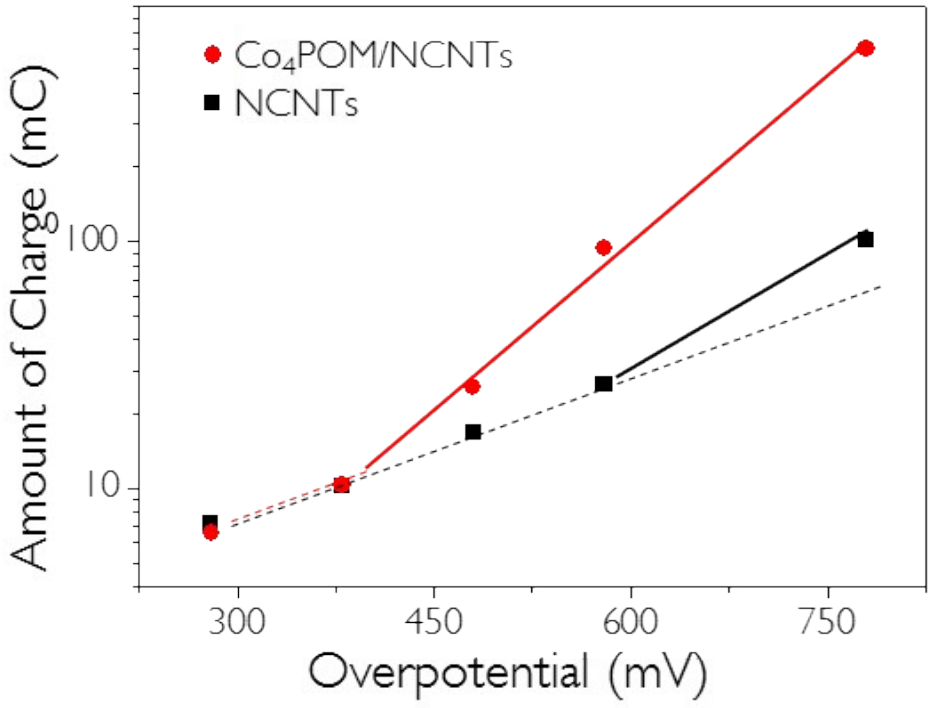

Fig. S16 The amount of charges generated from NCNTs (black) and the Co_4POM/NCNT hybrids (red) as a function of overpotential. Dotted and solid lines indicate the generated charges by capacitive and faradaic currents, respectively.

Table S5. A comparison of electrochemical performance of POM/Carbon nanomaterials based electrode for water oxidation.

System	Characteristic of catalytic system	pH	Over potential (V)	Tafel slope (mV decade^{-1})	Reaction time (s)	TOF (s^{-1})	Ref.
Co_4POM^a/NCNT	Catalyst on N-doped CNT	7.0	0.37	203	1800	0.211	This work
Co_4POM^a	Homogeneous catalyst with $[Ru(bpy)_3]^{2+}$] for stoichiometric oxidant	8.0	N/A ("a low overpotential for the water oxidation")	N/A	N/A	5	3
Ru_4POM^b	Homogeneous catalyst with Ce(IV)	0.6	N/A	N/A	7200	> 0.125	5
Ru_4POM^b/d-CNT	Catalyst on PAMAM[c] functionalized CNT	7.0	0.35	296	400	0.055	6
Ru_4POM^b/d-graphene	Catalyst on PAMAM [c] functionalized graphene	7.0	0.30	222	400	0.26	7
Ru_4POM^b-graphene	Catalyst on graphene modified glassy carbon electrode with 1 M $Ca(NO_3)_2$	7.5	N/A	N/A	400	2.70	8

[a] $Co_4POM = [Co_4(H_2O)_2(PW_9O_{34})_2]^{10-}$. [b] $Ru_4POM = [Ru_4(\mu\text{-}O)_4(\mu\text{-}OH)_2(H_2O)_4(\gamma\text{-}SiW_{10}O_{36})_2]^{10-}$. [c] PAMAM = polyamidoamine. [d] 2-aminoethyltrimethylammonium.

References

1. G. Kresse, J. Furthmuller, *Phys. Rev. B* 1996, **54**, 11169-11186.

2. Y. Liang, Y. Li, H. Wang, J. Zhou, J. Wang, T. Regier, H. Dai, *Nat. Mater.* 2011, **10**, 780-786.

3. Q. Yin, J. M. Tan, C. Besson, Y. V. Geletii, D. G. Musaev, A. E. Kuznetsov, Z. Luo, K. I. Hardcastle, C. L. Hill, *Science* 2010, **328**, 342-345.

4. W. Tang, E. Sanville, G. Henkelman, *J. Phys.: Condens. Matter.* 2009, **21**, 084204.

5. A. Sartorel, M. Carraro, G. Scorrano, R. D. Zorzi, S. Geremia, N. D. McDaniel, S. Bernhard, M. Bonchio, *J. Am. Chem. Soc.* 2008, **130**, 5006-5007.

6. F. M. Toma, A. Sartorel, M. Iurlo, M. Carraro, P. Parisse, C. Maccato, S. Rapino, B. R. Gonzalez, H. Amenitsch, T. Da Ros, L. Casalis, A. Goldoni, M. Marcaccio, G. Scorrano, G. Scoles, F. Paolucci, M. Prato, M. Bonchio, *Nat. Chem.* 2010, **2**, 826-831.

7. M. Quintana, A. M. Lopez, S. Rapino, F. M. Toma, M. Iurlo, M. Carraro, A. Sartorel, C. Maccato, X. Ke, C. Bittencourt, T. Da Ros, G. Van Tendeloo, M. Marcaccio, F. Paolucci, M. Prato, M. Bonchio, *ACS Nano* 2013, **7**, 811-817.

8. S.-X. Guo, Y. Liu, C.-Y. Lee, A. M. Bond, J. Zhang, Y. V. Geletii, C. L. Hill, *Energy Environ. Sci.* 2013, **6**, 2654-2663.